Korea-Australia Rheology Journal, Vol.25, No.4, pp.233-242 (November 2013) www.springer.com/13367
DOI: 10.1007/s13367-013-0024-7

On the yield stress of complex materials

F. Calderas[1,*], E. E. Herrera-Valencia[1], A. Sanchez-Solis[1], O. Manero[1], L. Medina-Torres[2], A. Renteria[2] and G. Sanchez-Olivares[3]

[1]*Instituto de Investigaciones en Materiales, Universidad Nacional Autónoma de México, A. P. 70-360, C. U. 04510, México, D. F., México*

[2]*Departamento de Ingeniería Química, Facultad de Química, Edificio "E". Universidad Nacional Autónoma de México, A. P. 70-360, C. U. 04510, México, D. F., México*

[3]*Departamento de materiales, CIATEC, A.C., Omega 201 37545 León, Guanajuato, México*

(Received March 6, 2013; final revision received September 4, 2013; accepted September 11, 2013)

In the present work, the yield stress of complex materials is analyzed and modeled using the Bautista-Manero-Puig (BMP) constitutive equation, consisting of the upper-convected Maxwell equation coupled to a kinetic equation to account for the breakdown and reformation of the fluid structure. BMP model predictions for a complex fluid in different flow situations are analyzed and compared with yield stress predictions of other rheological models, and with experiments on fluids that exhibit yield stresses. It is shown that one of the main features of the BMP model is that it predicts a real yield stress (elastic solid or Hookean behavior) as one of the material parameters, the zero shear-rate fluidity, is zero. In addition, the transition to fluid-like behavior is continuous, as opposed to predictions of more empirical models.

Keywords: Bautista-Manero-Puig model (BMP), yield Stress, rheological modeling, complex Fluids

1. Introduction

The yield stress of complex materials has been the object of a great deal of attention. The yield stress occurs when the shear stress becomes independent of the shear strain (constant value) and the system behaves as an elastic solid. However, for increasing strain rates, past a critical point (yield stress), the material flows. In some articles, the real yield stress is identified with the Bingham yield stress, namely, an asymptotic non-zero value of the stress as the shear rate tends to zero. On the other hand, the term "apparent yield stress" is identified with a very large zero-shear rate viscosity, but such behavior corresponds to a stress value of zero as the shear rate is zero.

A viscoplastic material exhibits little or no deformation up to a critical value of stress (the yield stress) above which the material flows. Concentrated suspensions of solid particles in Newtonian liquids exhibit yield stress followed by nearly Newtonian behavior. These materials are often called Bingham plastics. Various fluids of a practical interest, such as liquid foams, paints, droplet emulsions or high cholesterol blood, possess such elastoviscoplastic behavior.

Cheng (1985) observed that the stress in an intermediate range of shear rates almost becomes constant, but with increasing shear rates a Newtonian-like behavior occurs. The existence of an essentially horizontal region in a double-logarithmic plot of stress versus strain rate was considered the most satisfactory criterion for the existence of a yield stress. Other authors agree with this description (Evans, 1992).

Two-and three-parameter models predict the region of high shear rates for yielding materials. At intermediate shear rates, both the Bingham (Barnes, 1999) and the Herschel-Bulkley (Herschel and Bulkley, 1926; Bingham, 1922) models do well in predicting a flattening of the stress as a function of shear rate. One of the computational problems mentioned in the review article by Barnes (1999) is that the behavior of a Bingham or similar materials at the yield stress is in no way smooth and differentiable in a mathematical sense. Below the yield stress, the viscosity is infinite, and above, it is an asymptotically decreasing function of shear stress, usually approaching a constant value of viscosity as the stress becomes infinite. These problems can lead to inconsistencies in the numerical modeling of flow in complex geometries (Lipscomb and Denn, 1984), and difficulties in properly defining the boundaries between non-deforming '*solid*' zones and flowing '*liquid*' zones.

Abdali *et al.,* (1992) presented results from a simulation of entry and exit flows into a circular tube of a modified Bingham fluid which eliminated stress singularities, using Papanastasiou's extra exponential term (Papanastasiou, 1987). Papanastasiou (1987) introduced a slightly modified version of the Bingham plastic (Bingham, 1922), containing three fitting parameters. This model produces a continuous change from a solid to a

*Corresponding author: faustocg@unam.mx

fluid behavior of the material. It is obvious that the material can be well approximated uniformly at all levels of stress as a liquid that exhibits very high viscosity in the limit of low strain rates followed by a continuous transition to a Newtonian plateau. The approximation can be made more accurate at very small strain rates by means of a material parameter that controls the exponential growth of stress. Under Poiseuille flow, as the flow becomes more and more dominated by the yield stress, the velocity profile becomes more plug-like. This arises because the material deformation is restricted in the tube to just near the wall. Although this model is continuous and differentiable, it does not predict a real solid-like behavior.

Alternative models have been proposed to account for the real solid, Hookean behavior before yielding. The Houlsby and Puzrin (2002) and Isayev and Fan (1990) models predict extensions to the original Voigt-Kelvin or Maxwell-like behavior with added yield stresses. The Houlsby and Puzrin (2002) model predicts an elastic behavior before yielding, followed by a Kelvin-Voigt solid behavior at long times. Likewise, the Isayev model (Isayev *et al.,* 1990) predicts a Hookean elastic behavior before yielding but a viscous behavior after yielding. These models have the disadvantage that the solid-liquid transition is discontinuous. However, the real deformation at the transition is expected to be smooth, at least continuous. A constitutive equation for elastoviscoplastic materials has been proposed by Saramito (2007, 2009) which is continuous and differentiable, but again, it does not predict a real solid-like behavior.

To predict a solid behavior, a new version of the latter viscoplastic model was suggested, based on the Herschel-Bulkley (1926) viscoplastic model, with a power-law index $n > 0$. At low stresses, the material exhibits a real yield stress, whereas for a stress above a yield stress, the material exhibits a shear-thinning or shear-thickening behavior.

In summary, models that predict real solid behavior and a smooth transition to liquid-like behavior are mostly empirical. Elsewhere (Bautista *et al.,* 1999), a model that predicts several rheological responses observed in complex materials, has been shown to describe the yield stress (apparent and "real"). Constitutive equations that take into account the build-up and break down kinetics of a complex fluid structure during flow have been used to model several complex systems (Bautista *et al.,* 1999). In the present work, predictions of the BMP model are compared to those of the mentioned models. The model presented here is basically in agreement with predictions of the mentioned models, but with a more consistent physical basis. In addition, experimental results on concentrated solutions under simple shear and creep are also compared with predictions of the BMP model. These solutions exhibit yield stresses as a function of the concentration.

2. Theory

2.1. Rheological equation of state

For the suspension of solid particles in a Newtonian solvent, the BMP (Bautista *et al.,* 1999) model is described by the following equations:

$$\boldsymbol{\sigma} = \boldsymbol{\sigma}_{pp} + \boldsymbol{\sigma}_{ps} + \boldsymbol{\sigma}_{s} = \boldsymbol{\sigma}_{p} + \boldsymbol{\sigma}_{s} \tag{1}$$

where the three contributions to the total stress are those arising from the particle-particle interactions (subindex "pp"), particle-solvent interactions (subindex "ps") and the solvent (subindex "s") contribution, respectively. For the contributions of particle-particle and particle-solvent interactions (subindex "p"), respectively, the following equations apply:

$$\boldsymbol{\sigma}_{p} + \frac{1}{G_0 \varphi_p} \overset{\nabla}{\boldsymbol{\sigma}}_{p} = \frac{2}{\varphi_p} \mathbf{D} \tag{2}$$

$$\frac{d\varphi_p}{dt} = \frac{\varphi_0 - \varphi}{\lambda} + \mathbf{k}(\varphi_\infty - \varphi)\boldsymbol{\sigma} : \mathbf{D} \tag{3}$$

while for the Newtonian solvent:

$$\boldsymbol{\sigma}_{s} = 2\eta_s \mathbf{D} \,. \tag{4}$$

$\boldsymbol{\sigma}$ is the total stress tensor, $\mathbf{D}$ is the symmetric part of the velocity gradient tensor, φ is the fluidity (inverse of the viscosity η), $\varphi_0 (\equiv \eta_0^{-1})$ is the zero strain-rate fluidity, φ_∞ is the fluidity at high strain rates, G_0 is the shear modulus, λ is the structural characteristic time and k is a kinetic constant related to structure modification. The upper-convected derivative of the stress tensor is:

$$\overset{\nabla}{\boldsymbol{\sigma}} = \frac{D}{Dt}\boldsymbol{\sigma} - (\mathbf{L} \cdot \boldsymbol{\sigma} + \boldsymbol{\sigma} \cdot \mathbf{L}^{T}) \tag{5}$$

where $\mathbf{L}$ is the velocity gradient tensor. Eqs. 2 and 3 reduce to the upper-convected Maxwell model when $\varphi = \varphi_0$ and to the Oldroyd model (Oldroyd, 1947, 1950) when the solvent is included. These equations express that the non-linear viscoelastic processes contained in the Maxwell equation are coupled with an equation written in terms of the fluidity, which is itself a kinetic equation with a characteristic time related to structure formation λ and a destruction term related to structure modification with kinetic constant k proportional to the dissipation. This version of the model is a simple one which neglects effects derived from concentration gradients and shear-banding phenomena included in a general formulation derived from extended irreversible thermodynamics (García-Rojas *et al.,* 2009). It is assumed that Eqs. 2 and 3 apply to the particle-solvent contribution at short times and to the particle-particle interactions at longer times. Hence, the constitutive equations may be written as:

$$\boldsymbol{\sigma} = \boldsymbol{\sigma}_p + 2\eta_s \mathbf{D} \tag{6}$$

$$\boldsymbol{\sigma}_p + \frac{1}{G_0 \varphi_p} \overset{\nabla}{\boldsymbol{\sigma}}_p = \frac{2}{\varphi_p} \mathbf{D} \tag{7}$$

$$\frac{d\varphi_p}{dt} = \frac{1}{\lambda}(\varphi_0 - \varphi) + k(\varphi_\infty - \varphi)\boldsymbol{\sigma} : \mathbf{D} \tag{8}$$

$$\frac{1}{\varphi} = \frac{1}{\varphi_p} + \eta_s \tag{9}$$

where subindex p includes particle-particle and particle-solvent contributions.

2.2. Steady state

Under steady-state, Eq. 8 gives the following expression for the normalized dissipation:

$$k\lambda(\boldsymbol{\sigma} : \mathbf{D}) = \frac{\varphi - \varphi_0}{\varphi_\infty - \varphi}. \tag{10}$$

Clearly, the dissipation due to particle-solvent and particle-particle interactions is small at small strain rates ($\varphi \to \varphi_0$) and it is large as the fluidity approaches the solvent fluidity. In Eq. 7, in the limit when the fluidity is zero, integration in time leads to Hooke´s law of an elastic solid. As shown later, this limit corresponds to that of a real yield stress, identified with a stress plateau independent of the shear rate. In terms of the total stress, Eqs. 6-9 may be written as:

$$\overset{\nabla}{\boldsymbol{\sigma}} + \tau_R \boldsymbol{\sigma} = 2(1/\varphi + \eta_s)\mathbf{D} + 2\eta_s \tau_R \overset{\nabla}{\mathbf{D}} \tag{11}$$

$$\frac{d\varphi_p}{dt} = \frac{1}{\lambda}(\varphi_0 - \varphi_p/(1 + \eta_s\varphi_p)) + k(\varphi_\infty - \varphi_p/(1 + \eta_s\varphi_p))\boldsymbol{\sigma} : D \tag{12}$$

$$\tau_R = (\varphi_p G_0)^{-1}, \quad \eta_s \varphi_p < 1. \tag{13}$$

Clearly, the variable stress relaxation time approaches the Maxwell relaxation time as $\varphi \to \varphi_0$, and when the fluidity of the suspension attains its largest value φ_∞ (necessarily it must be smaller than the solvent fluidity) the relaxation time tends to zero. Under simple shear flow and neglecting normal stress effects, Eqs. 11-13 become:

$$\sigma + \tau_R \frac{d\sigma}{dt} = (1/\varphi_p + \eta_s)\dot{\gamma} + \eta_s \tau_R \frac{d\dot{\gamma}}{dt} \tag{14}$$

$$\frac{d\varphi_p}{dt} = \frac{1}{\lambda}(\varphi_0 - \varphi) + k(\varphi_\infty - \varphi)\sigma\dot{\gamma}. \tag{15}$$

Where $\dot{\gamma}$ is the shear rate and the non-linear terms in Eqs. 11 and 13, which generate normal stresses are not considered here. At steady state, Eqs. 14 and 15 may be combined to give:

$$(\varphi_0 k\lambda\sigma^2)\varphi_{ss}^2 + (1 - k\lambda\varphi_\infty\sigma^2)\varphi_{ss} + (-\varphi_0) = 0 \tag{16}$$

where

$$1/\varphi_{ss} = (1/\varphi_p + \eta_s)_{ss}. \tag{17}$$

Eq. 16 predicts shear-thinning behavior when $\varphi_\infty > \varphi_0$, shear-thickening when $\varphi_\infty < \varphi_0$ and Newtonian behavior when $\varphi_\infty = \varphi_0$. A near-plateau region is predicted in the limits of very low and very high shear rates, with a power-law behavior in the intermediate shear rates. In addition, a real yield stress is predicted when $\varphi_0 = 0$. The real yield stress implies an elastic solid (Hookean) behavior in the limit when the shear rate approaches zero, as in the Bingham viscoplastic model. Apparent yield is predicted for very small values of φ_0. From Eq. 16, the yield stress can be calculated when $\varphi_0 = 0$ in the region of very small shear rates. This gives:

$$\sigma_y = (k\lambda\varphi_\infty)^{-1/2} \tag{18}$$

Eqn. 16 may be solved for φ_{ss} to give:

$$\frac{\varphi_{ss}}{\varphi_\infty} = \frac{(\sigma_R^2 - 1) + \theta\lambda}{2\sigma_R^2} \tag{19}$$

where

$$\theta\lambda = \sqrt{(\sigma_R^2 - 1)^2 + 4\sigma_R^2(\varphi_0/\varphi_\infty)} \tag{20}$$

and the reduced yield stress is defined as:

$$\sigma_R = \frac{\sigma}{\sigma_y}. \tag{21}$$

The three material constants contained in the above equations $\{\varphi_\infty, \varphi_0, \sigma_y\}$ may be evaluated from independent rheometric measurements in steady and unsteady flows. The fluidities at lower and high shear rates $\{\varphi_\infty, \varphi_0\}$ can be estimated through experiments in steady shear flow. The structural time and elastic modulus $\{G_0, \lambda\}$ can be calculated by using linear oscillatory flow. The kinetic constant $\{k\}$ can be evaluated in stress relaxation experiments after steady shear flow; in this sense, the model does not contain fitting parameters (Calderas *et al.,* 2009; Herrera *et al.,* 2009, 2010; Calderas 2012).

3. Results

3.1. Flow curves behavior

As reported previously for the BMP model (Bautista *et al.,* 1999), in the case $\varphi_0 > 0$, the stress goes to zero as the applied shear rate goes to zero, except when $\varphi_0 = 0$; in this case, Bingham behavior is observed, corresponding to a real yield stress. Depending on the value of the shear stress, two cases are observed: a "real" yield stress (zero fluidity and a constant shear value independent on the shear rate) and an apparent yield (small enough but non-zero fluidity and shear stress dependent on the shear rate). The difference is only noticeable in a log-log plot (see Bautista *et al.,* 1999).

A first Newtonian region is predicted, ending at shear rates of order $G_0\varphi_0 = \lambda_0^{-1}$, and the onset for the yield stress corresponds to shear rates of order $\lambda_y^{-1} = G_0\varphi_\infty$. As $\varphi_0 \to 0$, λ_0^{-1} also tends to zero and the plateau extends to lower shear rates, up to the point where the first Newtonian region vanishes and gives way to a non-zero stress for vanishing shear rates (see Bautista *et al.,* 1999).This is the regime where the parameters of constitutive Eqs. 7 and 8 are dominated by a very small constant φ_0 and Eq. 7 tends to Hooke's law, the elastic solid behavior. As the elastic modulus G_0 grows, the material becomes a rigid solid (a solid that does not deform, except at considerable lengths of time). Likewise, shear rates of λ_y^{-1} order lie in the transition zone from yield to flow behavior. With respect to the characteristic time λ, which represents the material dynamic structure, it may vary in the range $\lambda_0 < \lambda < \lambda_\infty$.

3.2. Time dependent behavior (Creep)

In this case, the applied shear stress is σ_1 and remains at this value while the sample deforms as a function of time. Eqs. 4 and 5 give:

$$\frac{d\varphi}{dt} = \frac{\varphi_0 - \varphi}{\lambda} + k(\varphi_\infty - \varphi)\sigma_1^2\varphi \tag{22}$$

This equation may be solved with the initial condition $\varphi(t=0) = \varphi_i$, and with $\varphi(t\to\infty) = \varphi_{ss}$ (steady state fluidity). The solution is (see Appendix A):

$$\varphi(t) = \varphi_{ss} + \left[\left(\frac{\varphi_\infty}{\theta\lambda}\sigma_R^2 + \frac{1}{\varphi_i - \varphi_{ss}}\right)e^{\theta t} - \frac{\varphi_\infty}{\theta\lambda}\sigma_R^2\right]^{-1}. \tag{23}$$

The compliance is defined as:

$$J(\sigma,t) = \int_0^t \varphi(t)dt\,. \tag{24}$$

With Eq. (23) substituted into Eq. (24), the following expression for the compliance is obtained:

$$J(\varphi_0,\varphi_\infty,\varphi_i,k,\lambda,\sigma_1,t) = \varphi_{ss}t + \frac{1}{k\sigma_1^2}\mathrm{Ln}\left|1 + (\varphi_i - \varphi_{ss})\frac{k\sigma_1^2}{\theta}(1 - e^{-\theta t})\right| \tag{25}$$

where the steady state fluidity $\theta\lambda$, the reduced shear stress and yield stress are given by the Eqs. (18-20).

3.3.1. Behavior at long times

At long times, the exponential term in Eq. 23 dominates and upon integration of Eqn. 24, the following equation is obtained:

$$J(\sigma,t) = J_e^0 + \varphi_{ss}t \tag{26}$$

where the elastic compliance ($J_e^0 \equiv G_0^{-1}$) is given by:

$$J_e^0 = \frac{\lambda(\varphi_i - \varphi_{ss})}{\theta\lambda + \frac{(\varphi_i - \varphi_{ss})}{\varphi_\infty}\sigma_R^2}\,. \tag{27}$$

Eq. 26 represents a straight line with slope φ_{ss} and with ordinate J_e^0, the latter depending on the magnitude of the applied shear stress through Eq. 27. Several limits of Eqs. 25 and 27 are analyzed as follows.

Case A: $\sigma_R < 1$.

When the applied stress is very small and lower than the yield stress, $\theta\lambda \to 1, \varphi_{ss} \to \varphi_0 = 0$. Eq. 26 reduces to:

$$J = J_e^0 = \varphi_i\lambda \tag{28}$$

This primary creep region is given in terms of the initial fluidity and structural time scale. At long times, the compliance reaches a constant elastic contribution, as in the linear Kelvin-Voigt model, implying an elastic solid behavior. Hence, the elastic compliance in this case is identified with $\varphi_i\lambda$.

Case B: $\sigma_R = 1$

In this case $\varphi_{ss} \to \varphi_0 = 0, \theta\lambda \to 0$, and Eq. 26 reduces to:

$$J(\sigma,t) = \lambda\varphi_\infty\,. \tag{29}$$

The response at long times again tends to the limit of an elastic solid, with a larger asymptotic elastic compliance than that of case A.

Case C: $\sigma_R > 1$

For stresses larger than the yield stress, Eq. 25 applies, but for the particular case when the applied stress is very large, $\theta\lambda \to 1 + \sigma_R^2, \varphi_{ss} \to \varphi_\infty$ and the elastic compliance vanishes in this limit. Eq. 25 becomes:

$$J(\sigma,t) = \varphi_{ss}t = \varphi_\infty t\,. \tag{30}$$

3.3.2. Behavior at short times

At sufficiently short times, the exponential term in Eq. 23 may be linearized, and upon integration, the compliance is obtained in this limit as follows:

$$J(\sigma,t) = \varphi_i t\,. \tag{31}$$

This equation predicts an initial slope of all curves in Fig. 1, in which the compliance is plotted with time for increasing stress values. Eq. 31 also expresses that for times of order λ, the initial slope attains the value of the elastic compliance. In the limit $\varphi_{0'} \to 0$, a rigid solid behavior (a solid with very large modulus) is attained, *i.e.*, the compliance is nearly zero for all times (see Bautista *et al.,* 1999). When the initial slope in Eq. 31 is very large ($\varphi_i \to \varphi_\infty$) the compliance follows a behavior corresponding to an elastic solid, in which a steep slope at short times is followed by an asymptotic region at long times, the elastic compliance (Fig. 1 b, see Eq. 28).

For small applied stresses, below the yield stress (Fig. 1 a, $\sigma_R < 1$) there is a primary creep region at short times, corresponding to the initial elastic response, given by Eq.

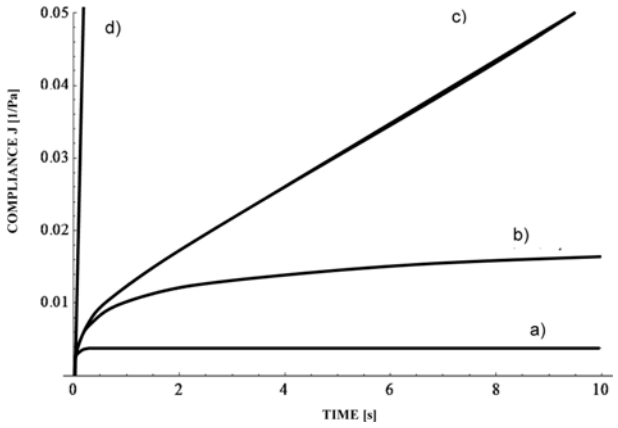

Fig. 1. Compliance as a function of time for 4 cases (λ=0.14 s, k=3.9×10^{-5} Pa^{-1}, φ_∞=10.5 Pas^{-1}): (a) Applied stress smaller than the yield stress ($\varphi_i=\varphi_\infty/10$, $\varphi_{ss}=0$); (b) applied stress equal to the yield stress ($\varphi_i=\varphi_\infty$, $\varphi_{ss}=0$); (c) applied stress larger than the yield stress ($\varphi_i=\varphi_\infty$, $\varphi_{ss}=\varphi_\infty/10$); (d) applied stress much larger than the yield stress ($\varphi_i=\varphi_\infty=\varphi_{ss}$).

31 ($\varphi_i<\varphi_\infty$). At long times, the sample stops deforming and the asymptotic elastic compliance is attained (Eq. 28). At the yield stress (Fig. 1b, $\sigma_R=1$) the initial slope is very large ($\varphi_i=\varphi_\infty$) followed by a larger asymptotic elastic compliance given by Eq. 29. For applied stresses larger than the yield stress (Fig. 1c, $\sigma_R>1$) Eq. 26, 28 and 31 apply. In Fig. 1c, the initial fluidity is set to $\varphi_i=\varphi_\infty$, followed by the steady-state fluidity with value $\varphi_{ss}=\varphi_\infty/10$. Finally, for stresses much larger than the yield stress (Fig. 1 d, $\sigma_R\gg1$), the initial and steady-state fluidities coincide ($\varphi_i=\varphi_{ss}=\varphi_\infty$) and in this case negligible primary creep is apparent.

3.3.3. Comparison with experiment

Predictions were compared with experiments made with Kaolin suspensions. Kaolin is a clay composed of silicates with mean particle size in the colloidal suspensions range (1-1000 nanometers), and concentrated suspensions in most cases present yield stresses. It is used in the pharmaceutical and paint industries as a dispersing agent or thickener, respectively.

The tests were made in a TA-Instruments AR-G2 stress-controlled rheometer. Sample preparation included mixing to homogenize the sample during 30 min with 0.05 wt% pectin using a *Lightin*® mixer. Only one concentration was considered: 60 wt%. The tests included steady simple shear in the range of 0.001 to 100 s^{-1} and creep experiments for various applied stresses at two temperatures (10 and 25°C) using parallel-plates 40 mm diameter with rough surfaces to avoid slipping at the solid-liquid interface. The creep tests were programmed to observe the response of the material at short and long times, up to the attainment of steady-state.

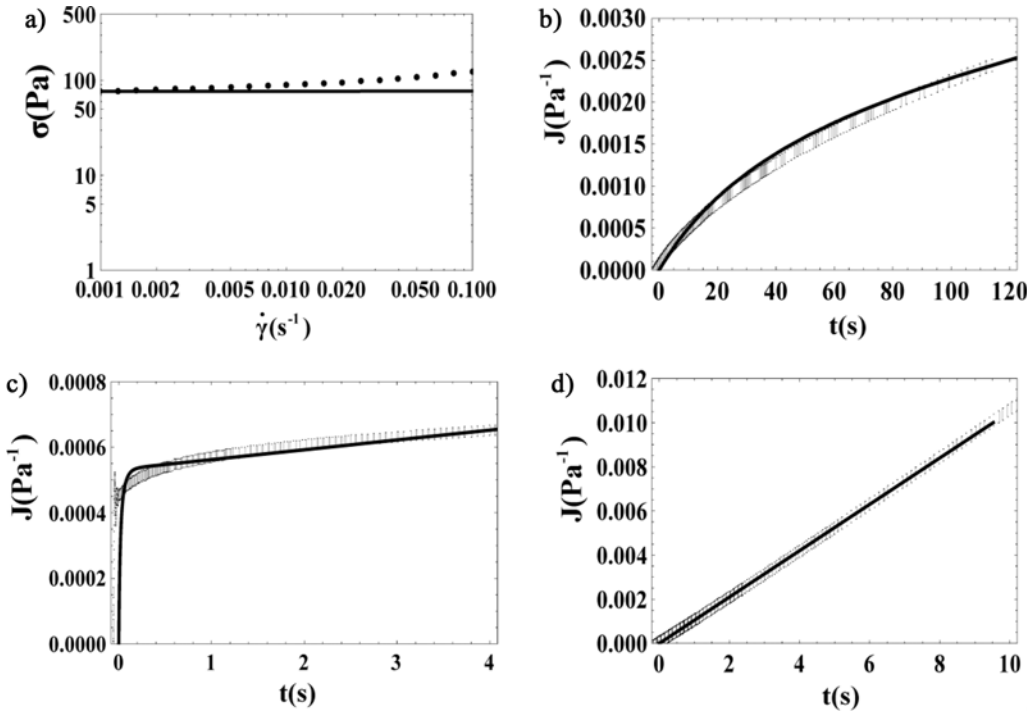

Fig. 2. (a) Steady state stress versus shear rate. 60 wt% Kaolin suspension in water at 10°C. (b) Compliance versus time. Applied stress: 77 Pa. (c) Compliance versus time. Applied stress is 80 Pa. (d) Compliance versus time. Applied stress is 130 Pa. Solid line: model predictions. Symbols: Experimental data.

Table 1. BMP model parameters used in the simulations for Figure 2

Figure	2a	2b	2c		2d
Mode	I	I	I	II	I
$\sigma_R(1)$	-	1	1.04	1.04	1.69
$\varphi_0(Pa{\cdot}s)^{-1}$	0	0	0	0	0
$\varphi_\infty\,(Pa{\cdot}s)^{-1}$	0.5	0.5	0.5	0.5	0.5
$\varphi_i(Pa{\cdot}s)^{-1}$	-	6×10^{-5}	0.018	0.018	1.05×10^{-3}
$\varphi_{ss}(Pa{\cdot}s)^{-1}$	-	8×10^{-6}	2×10^{-5}	1×10^{-5}	1.05×10^{-3}
$k(Pa)^{-1}$	0.0911	0.0911	0.6	0.6	0.0911
$\lambda(s)$	3.7×10^{-3}	4×10^{-3}	3.6×10^{-3}	1×10^{-3}	0.018
$J_e^0\,(Pa)^{-1}$	-	1.14×10^{-3}	5.5×10^{-5}	-	0

Two sets of data were collected at two temperatures (10 and 25°C) at 60 wt% concentration, in both steady state and creep flow. At 10°C, Fig. 2a shows the stress versus shear rate curve indicating the approach to a constant stress independent of the shear rate, as the shear rate decreases to very low values. In Figs. 2b, 2c and 2d the compliance as a function of time is shown for increasing applied stresses, where data and predictions are observed. The method by which model predictions are calculated, involve Eqs. 16-19 and 26. With the experimental value of the yield stress in Fig. 2a and φ_∞ obtained from the fitting of the flow curve using Eqs. 17-19, Eq. 16 renders the product $k\lambda$. The parameter λ is found independently, since creep flow data renders the initial and steady state fluidities from the initial and long time slopes of the compliance *curve*. The intercept (Eq. 27) gives the elastic compliance and the value of $\theta\lambda$ is found from the applied stress. Since a real yield stress is revealed in the flow curves, the predictions were made with $\varphi_0 = 0$.

As observed in Table 1, for Figs. 2b and 2d, a single mode is sufficient to predict the data, with exception of the curve produced with an applied stress slightly larger than the yield stress. In this case (Fig. 2c), two modes are included: the first one is assigned to particle-solvent interactions occurring at short times, and the second one operating in the long time range. The first mode should be included to predict the data in the short time range of the compliance curve.

In most cases, it was found that the steady state fluidity calculated from the flow curve (stress versus shear rate) given an applied stress does not coincide with that found from the creep curve at long times. The reason for this discrepancy is probably due to remaining slip at the solid-liquid interface, even when rough surfaces of the parallel plates were used. Nonetheless, we believe that this is evidence of the presence of slip in these experiments; further experiments (forthcoming reports) will deal with the use of other geometries (vane) to more effectively avoid slip in these systems. Due to slip, only at high applied stresses both fluidities coincide (see Fig. 2d).

At 25°C, Fig. 3 exhibits data and predictions of the yield

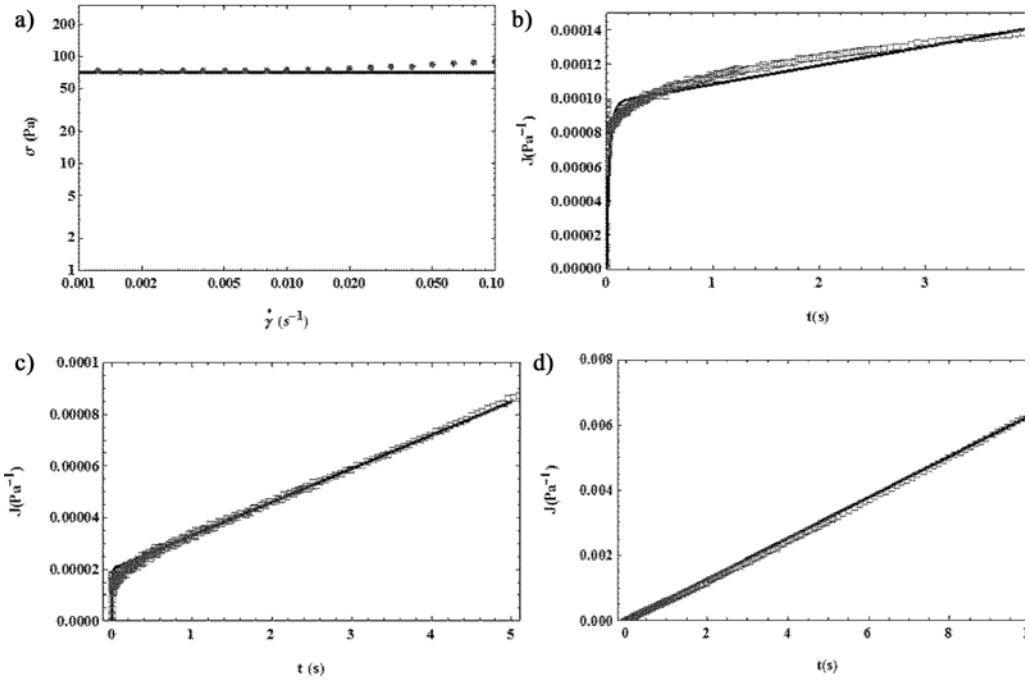

Fig. 3. (a) Steady state stress versus shear rate. 60 wt% Kaolin suspension in water at 25°C. (b) Compliance versus time. Applied stress: 70 Pa. (c) Compliance versus time. Applied stress is 90 Pa. (d) Compliance versus time. Applied stress is 130 Pa. Solid line: model predictions. Symbols: Experimental data.

Table 2. BMP model parameters used in the simulations for Figure 3

Figure	3a	3b		3c	3d
Mode	I	I	II	I	I
$\sigma_R(1)$	-	1.14	1.14	1.29	1.85
$\varphi_0(Pa{\cdot}s)^{-1}$	0	0	0	0	0
$\varphi_\infty\ (Pa{\cdot}s)^{-1}$	0.5	0.5	0.5	0.5	0.5
$\varphi_i(Pa{\cdot}s)^{-1}$	-	3.5×10^{-3}	3.5×10^{-3}	3.5×10^{-3}	6.3×10^{-4}
$\varphi_{ss}(Pa{\cdot}s)^{-1}$	-	1×10^{-5}	1×10^{-6}	1.3×10^{-5}	6.3×10^{-4}
$k(Pa)^{-1}$	0.116	0.6	0.6	0.116	0.116
$\lambda(s)$	3.5×10^{-3}	0.01	3.5×10^{-3}	4.4×10^{-3}	0.23
$J_e^0\ (Pa)^{-1}$	-	9.5×10^{-5}	-	1.98×10^{-5}	0

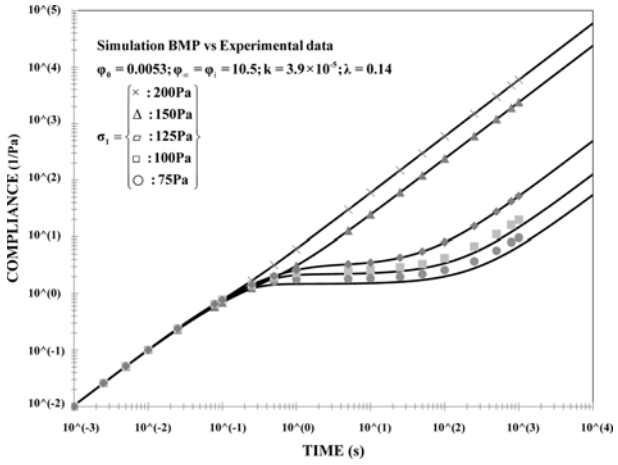

Fig. 4. Theoretical predictions of the BMP model for different applied shear stresses (solid lines) and experimental data (symbols) for a structural liquid (Catsup).

stress. Once again, for applied stresses slightly larger than the yield stress, two modes are necessary (see Table 2 and Fig. 3b).

A comparison of the model predictions with data published elsewhere (Caton and Baravian, 2008) is shown in Fig. 4. The theoretical predictions of the BMP model for different applied shear stresses and experimental data for a complex liquid (Catsup) are shown. At short times, the system shows a linear behavior, however for a critical time-value the system exhibits a monotonically increasing behavior followed by a second linear behavior with smaller slope at long times. Here, the system is dominated by the storage mechanism (elastic response), whereas at the highest value of the applied stress, the compliance shows a linear time response with slope given by Eq. 30. The experimental observations from Caton and Baravian (2008) are in good agreement with the BMP compliance predictions at high and intermediate time values for different applied shear stress. It is important to note that the theoretical predictions do not reproduce the experimental data at long times. It is thought that the multimodal version of the model could be more effective at long times. However, qualitatively the tendency of the data is reproduced well by the model.

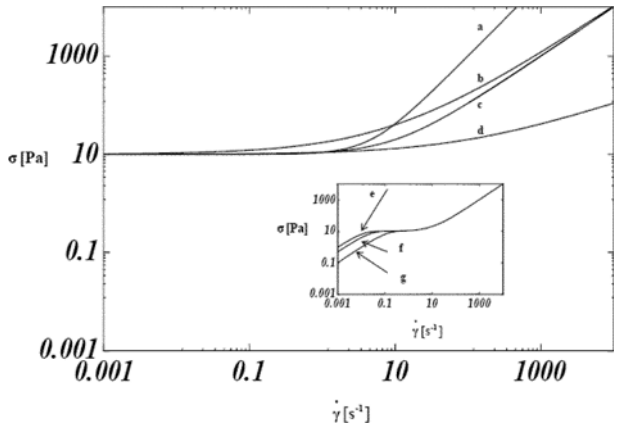

Fig. 5. Shear stress as a function of shear rate. Predictions of several models: (a) H.B. n = 0.5, σ_y=10. (b) Saramito. n = 0.5, σ_y=10. (c) Casson. σ_y=10. (d) Bingham, σ_y=10. (e, f, g) Papanastsiou, σ_y=10, n = 5, 10, 15.

4. Discussion

The BMP model predicts before yielding an initial response corresponding to Eq. 31 at short times ($J(\sigma,t) = \varphi_i t$) followed by an asymptotic region at long times given by Eq. 28, case A ($J(\sigma,t) = J_e^0 = \lambda\varphi_i$). A solid-like response after yielding ($\sigma_1 > \sigma_y$) may be predicted by case B of the BMP model. This is, for $\varphi_{ss} \to \varphi_0 = 0$ and at long times, $J(\sigma,t) = \varphi_\infty\lambda$, case B, describing a larger asymptote after yielding (since $\varphi_i \le \varphi_\infty$). At short times, the compliance may grow steeply according to $J(\sigma,t) = \varphi_\infty t$. This behavior agrees with predictions by the model by Houlsby and Puzrin (2002), which captures the behavior of saturated clays.

Another case is when the compliance grows with no bound (fluid-like behavior) according to the Oldroyd (or Maxwell) linear viscoelastic model, which may be reproduced by Eq. 26. This is in agreement with predictions of the Isayev and Fan (1990) model, which is known to describe the flow behavior of filled polymers. The behavior after yielding of the BMP model depends on the steady state fluidity, as in the linear Maxwell model (see case C) which may attain values between φ_0 and φ_∞. For stresses slightly larger than the yield stress, the slope of the compliance, the steady-state fluidity, is close to the zero shear-rate fluidity. When the stress is very high, the slope becomes φ_∞ with negligible elastic compliance, which apparently is not predicted by the Isayev and Fan (1990) model. Then, both models agree when the stress is not too high.

In Fig. 5, a comparison of predictions by several models

in the yield stress region is depicted. As observed, the "real" yield stress models predict an asymptotic region independent of the shear rate for vanishing shear rates (Bingham, 1922; Hershel and Bulkley, 1926; Saramito, 2009; Casson, 1959; Bautista *et al*., 1999). In the insets, models that predict "apparent" yield stresses are shown, illustrating the region at vanishing shear rates where the flow curves tend to a very high zero shear-rate viscosity (Papanastasiou, 1987; Saramito, 2007).

The BMP model complies with the rigid solid behavior before yielding of the Bingham (1922) or Herschel-Bulkley (1926) models; it predicts an elastic or viscoelastic solid behavior, as in the Houlsby and Puzrim (2002), Isayev and Fan (1990) or Saramito (2007, 2009) models, and finally, after yielding predicts a viscoelastic solid, Newtonian or fluid-like Oldroyd behavior (Oldroyd, 1947, 1950). As φ_0 tends to zero, the initial compliance complies with the limit of an elastic rigid solid, with negligible compliance. Kelvin-Voigt behavior is predicted for an initial fluidity tending to φ_∞ and a steady state fluidity $\varphi_0 = 0$. This is to be expected when the applied stress is close to the yield stress. For applied stresses larger than the yield stress, we expect a fluid-like behavior with slope larger than φ_0 for long times, and with the elastic compliance given by Eq. 28. As in the Oldroyd model, the primary creep is associated to the initial fluidity, or the solvent fluidity, that may be very large. Here, the initial fluidity may be also very large (φ_∞) which is of the order of the solvent fluidity.

5. Conclusions

Predictions of the BMP model were compared with those of other models intended to describe the yield stress of complex materials, and with experiments. The BMP model predicts a Hookean elastic-solid behavior independent of the shear rate for vanishing shear rates. In this context, it agrees with empirical models that predict a real yield stress, as the Bingham or Hershel-Bulkley models. Notwithstanding, for increasing strain rates above those of the yield stress, the behavior may be that of an asymptotic solid-like one (as in some of the mentioned models) or liquid-like, as in the Oldroyd and other quoted models. The BMP model in its single-mode or multi-mode versions, also describes experimental data of water-solid particle concentrated suspensions and data taken from the current literature. The model described here has a sound physical basis rather than empirical, which readily contributes to the understanding of complex flow behavior.

Acknowledgements

The authors wish to acknowledge the support of the National Council of Science and Technology of Mexico (CONACYT) Projects 162980 and 100195. EEHV gratefully acknowledges financial fellowship support (Postdoctoral Grant 147870) and the Canadian Government through Foreign Affairs and International Trade Canada (DFAIT). FC gratefully acknowledges financial fellowship support (Postdoctoral Grant Conacyt Project 100195)

Appendix A

In this appendix, the fluidity and compliance as functions of the reduced shear stress are obtained. In this case, the shear stress on the fluid is suddenly changed from σ_0 to σ_1 and remains at the latter value for subsequent times. For a simple shear flow and neglecting normal stresses, the following expressions are obtained:

$$\frac{d\varphi}{dt} = \frac{\varphi_0 - \varphi}{\lambda} + k\varphi(\varphi_\infty - \varphi)\varphi\sigma_1^2 . \tag{A-1}$$

This equation, in turn, can be written in the form of the Ricatti equation, *i.e.*

$$\frac{d\varphi}{dt} = -k\sigma_1^2\varphi^2 + \left(k\sigma_1^2\varphi_\infty - \frac{1}{\lambda}\right)\varphi + \frac{\varphi_0}{\lambda} . \tag{A-2}$$

At steady state, the time derivative of the fluidity is equal to zero, *i.e.* $d\varphi/dt = 0$, the above equation can be written in the following form:

$$(\lambda k\sigma_1^2)\varphi_{ss}^2 + (1 - \lambda k\sigma_1^2\varphi_\infty)\varphi_{ss} + (-\varphi_0) = 0 \tag{A-3}$$

which is quadratic in the fluidity. The positive root is given by the following expression

$$\frac{\varphi_{ss}}{\varphi_\infty} = \frac{\lambda k\varphi_\infty\sigma_1^2 - 1 + \sqrt{(\lambda k\varphi_\infty\sigma_1^2 - 1)^2 + 4(\varphi_0/\varphi_\infty)\lambda k\varphi_\infty\sigma_1^2}}{2\lambda k\varphi_\infty\sigma_1^2} . \tag{A-4}$$

Performing the change of variable $\varphi(t) = \varphi_{ss} + \varphi_t(t) = \varphi_{ss} + y^{-1}(t)$ with the initial condition $\varphi(t=0) = \varphi_i$ where φ_i is the fluidity corresponding to the initial stress σ_0, and $\varphi(t\to\infty)\to\varphi_{ss}$, it yields:

$$\frac{d}{dt}(\varphi_{ss} + y^{-1}(t)) = -k\sigma_1^2(\varphi_{ss} + y^{-1}(t))^2$$

$$+\left(k\sigma_1^2\varphi_\infty - \frac{1}{\lambda}\right)(\varphi_{ss} + y^{-1}(t)) + \frac{\varphi_0}{\mu} . \tag{A-5}$$

Taking the time derivative of the above expression:

$$\frac{dy(t)}{dt} = \underbrace{\left[k\sigma_1^2\varphi_{ss}^2 + \left(\frac{1}{\lambda} - k\sigma_1^2\varphi_\infty\right)\varphi_{ss} - \frac{\varphi_0}{\lambda}\right]}_{0} y^2(t)$$

$$+\left[2k\sigma_1^2\varphi_{ss} + \frac{1}{\lambda} - k\sigma_1^2\varphi_\infty\right]y(t) + k\sigma_1^2 . \tag{A-6}$$

In Eqn. (A-6), the first bracket contains the steady state fluidity and it is equal to zero (see Eqn. (A-3). Finally, the system is reduced to the following linear equation

$$\frac{dy(t)}{dt} = \left[2k\sigma_1^2\varphi_{ss}^2 + \frac{1}{\lambda} - k\sigma_1^2\varphi_\infty\right]y(t) + k\sigma_1^2 = \theta y(t) + k\sigma_1^2 \tag{A-7}$$

where $\theta = 2k\sigma_1^2\varphi_{ss} + \frac{1}{\lambda} - k\sigma_1^2\varphi_\infty$ is the inverse of a time scale associated to the applied shear stress and kinetic, viscous and structural processes. Finally, the linear differential equation is given by

$$\frac{dy(t)}{dt} = \theta y(t) + k\sigma_1^2 . \quad \text{(A-8)}$$

Integrating Eqn. (A-8) with the initial condition $y(t=0) = y(0)$

$$y(t) = \frac{1}{\theta}e^{\theta t}(\theta y(0) + k\sigma_1^2) - \frac{k\sigma_1^2}{\theta} . \quad \text{(A-9)}$$

The fluidity is finally given by

$$\varphi(t) = \varphi_{ss} + \frac{1}{y(t)} = \varphi_{ss} + \frac{1}{\left(\frac{1}{\varphi_i - \varphi_{ss}} + \frac{k\sigma_1^2}{\theta}\right)e^{\theta t} - \frac{k\sigma_1^2}{\theta}} . \quad \text{(A-10)}$$

In Eqn. (A-10) the following initial condition in terms of the fluidity was used

$$y(0) = \frac{1}{\varphi(0) - \varphi_{ss}(0)} = \frac{1}{\varphi_i - \varphi_{ss}(0)} . \quad \text{(A-11)}$$

Compliance

The compliance is calculated using the following integral

$$J(t) = \int_0^t \varphi(\xi)d\xi = \int_0^t \left(\varphi_{ss} + \frac{e^{-\theta\xi}}{(1/\varphi_i - \varphi_{ss} + k\sigma_1^2/\theta) - (k\sigma_1^2/\theta)}\right)d\xi . \quad \text{(A-12)}$$

Substituting the fluidity (Eqn. A-10) into Eqn. A-12, with the following variable change:

$u(\xi) = (1/\varphi_i - \varphi_{ss} + k\sigma_1^2/\theta) - (k\sigma_1^2/\theta)e^{-\theta\xi}$, we have:

$$J(t) = \varphi_{ss}t + \frac{1}{k\sigma_1^2}\mathrm{Ln}\left|1 + (\varphi_i - \varphi_{ss})\frac{k\sigma_1^2}{\theta}(1 - e^{-\theta t})\right| . \quad \text{(A-13)}$$

Equation A-13 can be simplified as the following form:

$$J(\sigma_R, \varphi_0, \varphi_\infty, \lambda, t) =$$

$$\lambda\varphi_\infty\left(\frac{\varphi_{ss}}{\varphi_\infty}(t/\lambda) + \frac{1}{\sigma_R^2}\mathrm{Ln}\left|1 + \left(1 - \frac{\varphi_{ss}}{\varphi_\infty}\right)\frac{\sigma_R^2}{\theta\lambda}(1 - e^{-\theta\lambda(t/\lambda)})\right|\right) \quad \text{(A-14)}$$

where:

$$\frac{\varphi_{ss}}{\varphi_\infty} = \frac{\sigma_R^2 - 1 + \sqrt{(\sigma_R^2 - 1)^2 + 4(\varphi_0/\varphi_\infty)\sigma_R^2}}{2\sigma_R^2} \quad \text{(A-15)}$$

$$\theta\lambda = \sqrt{(\sigma_R^2 - 1)^2 + 4(\varphi_0/\varphi_\infty)\sigma_R^2} \quad \text{(A-16)}$$

$$\sigma_R = \frac{\sigma_1}{\sigma_y} = \frac{\sigma_1}{1/\sqrt{k\lambda\varphi_\infty}} . \quad \text{(A-17)}$$

In Eqn. (A-14) the initial fluidity $\varphi_i = \varphi(0)$ takes the value of the fluidity at high shear rate, *i.e.* $\varphi_i = \varphi_\infty$.

Nomenclatures

J	Compliance [Pa^{-1}]
J_e^0	Elastic compliance [Pa^{-1}]
G_0	Elastic module [Pa]
k	Kinetic constant [Pa^{-1}]
R	Radius of the pipe [m]
$\Delta p/L$	Pressure gradient [Pa/m]

Tensors

$\boldsymbol{\sigma}_{pp}$	Particle-particle shear stress tensor [Pa]
$\boldsymbol{\sigma}_{ps}$	Particle-solvent shear stress tensor [Pa]
$\boldsymbol{\sigma}_s$	Solvent stress tensor [Pa]
D	Shear strain tensor [s^{-1}]
$\boldsymbol{\sigma}$	Total shear stress tensor
$\boldsymbol{\sigma}_p$	Total particle shear stress tensor [Pa]

Greeks

λ_0^{-1}	Characteristic shear strain at Newtonian region [s^{-1}]
λ_y^{-1}	Characteristic shear strain at yield stress region [s^{-1}]
$\theta\lambda$	Dimensionless time [$Pa^{-1}s^{-1}$]
φ_0	Fluidity at low shear stress [$Pa^{-1}s^{-1}$]
φ_∞	Fluidity at high shear stress [$Pa^{-1}s^{-1}$]
φ_i	Initial fluidity [$Pa^{-1}s^{-1}$]
τ_R	Maxwell time [s]
λ_0	Maxwell relaxation time at low shear rate [s]
λ_∞	Maxwell relaxation time at high shear rate [s]
φ_p	Particle fluidity function [$Pa^{-1}s^{-1}$]
σ_R	Reduced shear stress [1]
λ	Structural relaxation time [s]
$\dot{\gamma}$	Shear strain scalar [s^{-1}]
η_s	Solvent viscosity [Pa s]
φ_{ss}	Steady state fluidity [$Pa^{-1}s^{-1}$]
σ_y	Yield stress [Pa]

Other symbols

(:)	Double dot tensorial product, Section 2.1
Exp	Exponential function [1]
$\int_r^R$	Integral [1]
<	Less than one [1]
D/Dt	Material derivative [s^{-1}]
<	More than one [1]
>>	Much more than one [1]
∇	Nabla operator [m^{-1}]

$\rightarrow$	Tends to [1]
$\sqrt{}$	Square root [1]
d/dt	Time derivative
dt	Time differential

Subscripts

e	Refers to the elastic contribution
∞	Refers to high shear strain deformations
s	Refers to the solvent contribution
ss	Refers to the steady-state contribution
o	Refers to the elastic module and low high shear rate
p	Refers to the particle interaction
pp	Refers to the particle-particle interaction
R	Refers to the reduced yield streess
ps	Refers to the particle-solvent interaction
y	Refers to the yield-stress regime

Superscripts

T	Transpose of a matrix

Abreviations

BMP	Bautista-Manero-Puig model
UME	Upper-convective Maxwell equations
CD	Codeformational time derivative

References

Abdali, S.S., E. Mitsoulis and N.C. Markatos, 1992, Entry and exit flows of Bingham fluids, *J. Rheol.* **36**, 389-407.

Barnes, H.A., 1999, The yield stress—a review —everything flows? *J. Non-Newtonian Fluid Mech.* **81**, 133-178.

Bautista, F., J.M. De Santos, J.E. Puig and O. Manero, 1999, Understanding thixotropic and antithixotropic behavior of viscoelastic micellar solutions and liquid crystalline dispersions. The model, *J Non-Newton Fluid Mech.* **80**, 93-113.

Bingham, E.C., 1922, *Fluidity and Plasticity*, McGraw-Hill, New York.

Calderas, F., 2012, *Reología en flujo transitorio de la mezcla de nanocompuestos Pet-Pen- Montmorillonita*, Ph.D. thesis, División de estudios de Posgrado de la Facultad de Química, Universidad Nacional Autónoma de México, México.

Calderas, F., A. Sánchez-Solís, A. Maciel and O. Manero, 2009, The transient flow of the PEN-Montmorillonite clay Nanocomposite, *Macromol Symp.* 283-284, 354-360.

Casson, N., 1959, *A flow equation for pigment oil suspensions of printing type ink, in Rheology of disperse System*, Mill, C.C. (ed.), Pergamon Press, Oxford.

Caton, F., C. Baravian, 2008, Plastic behavior of some yield stress fluids: from creep to long-time yield, *Rheol. Acta* **47**, 601-607.

Cheng, D.C.H., 1985, *Yield stress: a time-dependent property and how to measure it*, Report No. LR 540 (MH), Warren Spring Laboratory, Department of Industry, UK.

Evans, I.D., 1992, Letter to the editor: on the nature of the yield stress, *J. Rheol.* **36**, 1313-1316.

García-Rojas, B., F. Bautista, J.E. Puig and O. Manero, 2009, Thermodynamic approach to rheology complex fluids: Flow-concentration coupling, *Phys. Rev E.* **80**, 036313/1-036313-12.

Herrera, E.E., F. Calderas, F., A.E. Chavez and O. Manero, 2010, Study of the pulsating flow of a worm-like micellar solution, *J. Non-Newtonian Fluid Mech.* **165**, 174-183.

Herrera, E.E., F. Calderas, A.E., Chávez, O. Manero and B. Mena, 2009, Effect of random longitudinal vibration pipe on the Poiseuille-flow of a complex liquid, *Rheol. Acta* **48**, 779-800.

Herschel, W.H., and T. Bulkley, 1926, Measurement of consistency as applied to rubber-benzene solutions, *Am. Soc. Test Proc.* **26**, 621-633.

Houlsby, G.T. and A.M. Puzrin, 2002, Rate-dependent plasticity models derived from potential functions, *J. Rheol*. **46**, 113-126.

Isayev, A. and X. Fan, 1990, Viscoelastic plastic constitutive equation for flow of particle filled polymers, *J. Rheol.* **34**, 35-54.

Lipscomb, G.G., and M.M. Denn, 1984, Flow of Bingham fluids in complex geometries, *J. Non-Newton Fluid Mech*. **14**, 337-346.

Oldroyd, J.G., 1947, A rational formulation of the equation of plastic flow for a Bingham solid, *Proc. Camb. Phil. Soc*. **43**, 100-105.

Oldroyd, J.G., 1950, On the formulation of rheological equation of state, *Proc. Roy. Soc. Lond. A,* **200**, 525-541.

Papanastasiou, T.C., 1987, Flows of materials with yield, *J. Rheol,* **31**, 385-404.

Saramito, P., 2007, A new constitutive equations for elastoviscoplastic fluid flows, *J. Non-Newton Fluid Mech.* **145**, 1-14.

Saramito, P., 2009, A new elastoviscoplastic model based on the Herschel-Bulkley viscoplastic model, *J. Non-Newton Fluid Mech.* **158**, 154-161.